

Research Paper

Research on the Motion Features Model for Underwater Targets with Multiple Highlights and Multiple Micro-Motion Forms

Tongjing SUN*, Zihan ZHOU, Dongliang PENG

*Department of Automation
Hangzhou Dianzi University, Xiasha Higher Education Zone
Hangzhou, China*

*Corresponding Author e-mail: stj@hdu.edu.cn

(received October 24, 2020; accepted April 2, 2020; published online February 26, 2024)

Motion characterization, including Doppler and micro-Doppler, is crucial for the detection and identification of high-speed underwater targets. Under high-frequency and short-range conditions, underwater targets cannot be simply regarded as single highlight targets as they exhibit a complex structure with multiple scattering centers accompanied by distinct micro-motions. To address this multi-highlight and multi-micro-motion scenario, a model is proposed to characterize the motion features of underwater targets. Firstly, a mathematical model is established to represent the micro-Doppler features based on the single-highlight model. Subsequently, considering the overlap of multiple highlight echoes caused by the high-speed translation of the target and the long pulse detection signal, precise representation is achieved by setting motion positions and calculating time delays within the model. The results represent the echoes of moving targets with multiple highlights and micro-motions. Finally, a time-frequency analysis method is employed to extract motion features and estimate target parameters, thereby validating the accuracy and effectiveness of the proposed model. This research provides a theoretical foundation for the modeling of underwater moving targets.

Keywords: micro-motion; complex motion; micro-Doppler; underwater micro-motion model; multi-highlight model.



Copyright © 2024 The Author(s).
This work is licensed under the Creative Commons Attribution 4.0 International CC BY 4.0
(<https://creativecommons.org/licenses/by/4.0/>).

1. Introduction

Existing studies have shown that underwater targets, during navigation or operational activities, exhibit periodic micro-motions such as vibrations and rotations alongside their translation (CLEMENTE *et al.*, 2013; HANIF *et al.*, 2022). Micro-Doppler features, serving as a crucial representation of target motion states, are particularly important in high-speed target detection. By extracting micro-Doppler features from complex echo signals, it is possible to estimate motion parameters of the high-speed target's micro-motion components, which is of great significance for target detection and identification.

In the field of radar detection, extensive research has been conducted on target micro-motion features, micro-motion feature extraction, and classification, leading to valuable achievements (CLEMENTE *et al.*, 2013; HANIF *et al.*, 2022). CHEN *et al.* (2003)

elucidated the frequency modulation effect caused by target micro-motion, known as micro-Doppler. Micro-Doppler features have been used for classifying various human activities. By using raw micro-Doppler signatures as features, detection and recognition of various human activities can be achieved (KIM, LING, 2009; KIM, MOON, 2016). WANG *et al.* (2023) employed time-frequency analysis to extract micro-Doppler features from radar signals to identify the indoor activities of elderly people, enabling an effective assessment of potential risks in their daily routines. ZHAO and SU (2023) decomposed Doppler signals from the echo of small unmanned aerial vehicles based on the micro-Doppler effect of rotating targets. They further extracted motion parameters from the residual rotating signals, achieving efficient identification of LSS UAVs. In addition to civilian applications, relevant research has also been conducted in the military domain. For instance, based on the estimation of

target micro-motion parameters, the identification of warheads has been accomplished, taking into account the different forms of target micro-motions (GAO *et al.*, 2010; HAN, FENG, 2020; ZHANG *et al.*, 2023).

In underwater acoustics, most research has concentrated on estimating motion parameters and position parameters of targets through Doppler parameters, enabling measurements such as velocity and range estimation (XU, 2016; TANG *et al.*, 2020). ZHANG *et al.* (2018) proposed a method based on frequency-difference-of-arrival measurements to accurately infer the position and velocity of underwater targets by considering the Doppler effect. GONG *et al.* (2020) introduced a low-complexity Doppler estimation algorithm to estimate the Doppler frequency shift and achieve localization of autonomous underwater vehicles. YANG *et al.* (2023) estimated the Doppler frequency shift to obtain the motion states of scatterers and then fused the motion features to accurately identify multiple moving scatterers within the same beam. Regarding micro-Doppler feature research, KASHYAP *et al.* (2015) simulated underwater vehicles with rotating propellers using sonar and radar detection. Employing time-frequency analysis to extract micro-Doppler features, the author confirmed that micro-Doppler features can be used for target identification. However, the presented simulation models lack generality. KULHANDJIAN *et al.* (2020) classified and recognized the swimming postures of humans on the water surface using acoustic micro-Doppler features. WU *et al.* (2022) simulated the motion features of composite targets with translational and micro-motion components, using a single-highlight model, and obtained the target's motion features through time-frequency analysis. KOU and FENG (2022) focused on targets with various micro-motion forms in a static state. The author separated multi-point echoes and extracted the micro-motion features of each highlight by constructing a redundant dictionary and sparse decomposition. SAFFARI *et al.* (2023) effectively selected features by extracting micro-Doppler features to distinguish and identify the propellers of various underwater target models (in stationary states) based on their different models and motion states.

Based on the above, most of the existing research models primarily consider micro-motion features in a stationary state and perceive the target as a single highlight structure. However, in actual underwater operational scenarios, targets often exhibit a combined motion pattern of translation and micro-motion, typically presenting complex structures with multiple scattering centers. For instance, in the case of a torpedo moving at high speed underwater, the tail fin undergoes a rotational motion and the engine compartment exhibits vibration. In light of this scenario, this paper builds upon the highlight model and establishes a motion characteristic model that incorporates multi-

ple highlight and micro-motions for combined translation and micro-motion. The feature parameters are extracted using time-frequency analysis methods to verify the correctness and effectiveness of the established model.

2. Mathematical model of micro-motion features based on single highlight

The single-highlight model for underwater targets (TANG, 1994) assumes that the relative distance between a moving target and the sonar remains constant during the pulse width of the transmitted signal. However, when underwater targets exhibit high-speed translation along with micro-motion, such as rotation and vibration, the position of the target's highlights changes not only due to translation but also due to micro-motion. This results in significant changes in the relative distance between the sonar and the target, which should be represented as an instantaneous distance $\mathbf{R}(t)$.

Assuming the transmitted signal is a long pulse signal:

$$p(t) = p_0(t)e^{-j2\pi ft}, \quad (1)$$

where $p_0(t)$ is the envelope of the signal and f is the carrier frequency.

During the pulse width of the transmitted signal illuminating the target, the highlight of the target is established as a dynamic model, represented as a vector indicating the relative distance $\mathbf{R}(t)$.

The vector distance relationship between the sonar and the micro-motion target is illustrated in Fig. 1. The sonar is located at the origin O of the coordinate system (x, y, z) and remains stationary. At time $t = 0$, the highlight of the target is located at the origin O_1 of the coordinate system (x_1, y_1, z_1) , which is a translation of the (x, y, z) coordinate system. The initial distance vector between the sonar and the target is denoted as \mathbf{R}_0 . The highlight moves uniformly with a velocity vector \mathbf{V} , and simultaneously, the micro-motion of the highlight introduces a distance change vector $\mathbf{M}(t)$. $\mathbf{M}(t)$ varies depending on the specific micro-motion pattern.

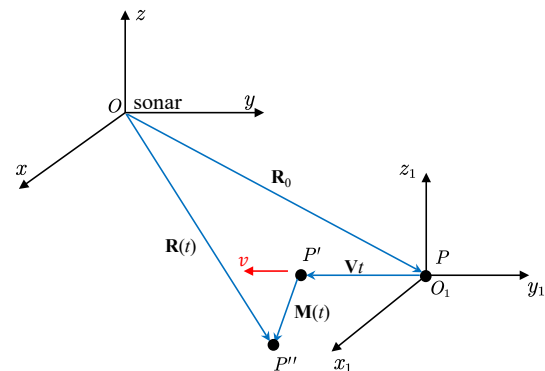


Fig. 1. Sonar and micro-motion target vector relationship.

The motion of the target can be decomposed into two stages: first, the target moves from point P to point P' , where the vector distance of this segment is equal to the translational velocity vector multiplied by time; then, based on the micro-motion pattern, it moves from point P' to point P'' , where the vector distance of this segment varies based on the form of infinitesimal motion. By adding these vectors together, we can obtain the instantaneous distance $\mathbf{R}(t)$:

$$\mathbf{R}(t) = \|\mathbf{R}_0 + \mathbf{V}t + \mathbf{M}(t)\|. \quad (2)$$

According to the highlight model theory, the time delay τ can be expressed as:

$$\tau = \frac{2\mathbf{R}(t)}{c}. \quad (3)$$

The echo signal expression is:

$$\begin{aligned} s(t) &= Ap_0 \left(t - \frac{2\mathbf{R}(t)}{c} \right) e^{-j2\pi f \left(t - \frac{2\mathbf{R}(t)}{c} \right)} e^{j\varphi} \\ &= Ap_0 \left(t - \frac{2\mathbf{R}(t)}{c} \right) e^{-j2\Phi(\mathbf{R}(t))} e^{j\varphi}, \end{aligned} \quad (4)$$

where A is the amplitude of the echo from the highlight, φ is the phase change at the formation of the echo, and $\Phi(\mathbf{R}(t))$ is the phase of the echo signal. By taking the derivative of the phase, we can obtain the instantaneous frequency:

$$f_t = \frac{1}{2\pi} \frac{d\Phi(\mathbf{R}(t))}{dt} = f - \frac{2f}{c} \frac{d\mathbf{R}(t)}{dt} = f - f'_t, \quad (5)$$

$$f'_t = f_d + f_{md} = \frac{2f}{c} [\mathbf{V}^T \cdot \mathbf{n}] + \frac{2f}{c} \left[\frac{d}{dt} (\mathbf{M}(t)) \right]^T \cdot \mathbf{n}, \quad (6)$$

where $\mathbf{n} = (\mathbf{R}_0 + \mathbf{V}t + \mathbf{M}(t)) / \|\mathbf{R}_0 + \mathbf{V}t + \mathbf{M}(t)\|$ is the unit vector of \mathbf{OP}'' , and since the initial distance is much larger than the distance generated by the target within one pulse period, we can approximate the unit vector of \mathbf{OP}'' as the unit vector of \mathbf{OP} , denoted as $\mathbf{n} \approx \mathbf{n}_p = \mathbf{R}_0 / \|\mathbf{R}_0\|$.

From the above derivation, we can see that $f_d = \frac{2f}{c} [\mathbf{V}^T \cdot \mathbf{n}]$ is the Doppler frequency shift, indicating that the echo signal form with Doppler frequency shift can be obtained through the dynamic representation of time delay. On the other hand, $f_{md} = \frac{2f}{c} \left[\frac{d}{dt} (\mathbf{M}(t)) \right]^T \cdot \mathbf{n}$ is the frequency shift caused by the frequency modulation resulting from micro-motion, known as the micro-Doppler frequency shift. Its essence is similar to the Doppler features, as both are caused by the change in the relative distance between the sonar and the target due to the target's motion, which leads to changes in the echo phase.

3. Motion features model for underwater targets with multiple highlights and micro-motion forms

For complex volumetric targets, a single highlight is insufficient to encompass their multifaceted

features. Therefore, it is necessary to consider them as a collection of multiple highlights, each exhibiting diverse micro-motion patterns. Taking a high-speed moving torpedo target as an example, a composite motion feature model is constructed to encompass multiple highlights and their different micro-motion patterns.

The torpedo is in a high-speed state underwater. Consider a five-highlight model for the torpedo. The head of the torpedo represents a stationary highlight without any micro-motion. The middle section contains an engine that causes mechanical vibrations in the body. Finally, the tail of the torpedo consists of three propeller blades that can be seen as three highlights rotating around the rear of the body.

The geometric relationship between the torpedo target and the observing sonar is illustrated in Fig. 2. Parts A, B, and C in Fig. 2d correspond to Figs. 2a–c, respectively. The observing sonar is located at the origin O of the sonar coordinate system (x, y, z) . Each highlight has its independent coordinate system relative to the sonar coordinate system, denoted as (x_1, y_1, z_1) , (x_2, y_2, z_2) , and (x_3, y_3, z_3) . These coordinate systems are translations of the sonar coordinate system (x, y, z) . The distribution and motion of these highlights are as mentioned above, representing the head, middle, and tail of the target, respectively. The highlight representing the middle section undergoes harmonic vibrations, with the origin O_2 of its coordinate system as the center of oscillation. The three highlights representing the tail section rotate around the origin O_3 of their coordinate system, with the y -axis as the rotation axis. They rotate with the same radius and angular velocity. The initial positions of these highlights in the coordinate system (x_3, y_3, z_3) are different. The entire target moves uniformly along the negative y -axis direction with a speed of v .

For a stationary highlight, as shown in Fig. 2a, the position of the highlight at the initial moment is P , which is located at the origin O_1 of the target coordinate system (x_1, y_1, z_1) . Its position vector in the sonar coordinate system (x, y, z) is $\mathbf{R}_1 = (X_1, Y_1, Z_1)^T$, and the initial azimuth and pitch angles are α_1 and β_1 , respectively. The radial unit vector of the sonar to the target is:

$$\mathbf{n}_p = \mathbf{R}_1 / \|\mathbf{R}_1\| = (\cos \alpha_1 \cos \beta_1, \sin \alpha_1 \cos \beta_1, \sin \beta_1)^T. \quad (7)$$

The velocity vector of the highlight is $\mathbf{V} = (0, v, 0)^T$. The instantaneous distance and echo signal expression of the highlight are:

$$\mathbf{R}_1(t) = \|\mathbf{R}_1 + \mathbf{V}t\| = \sqrt{X_1^2 + (Y_1 + vt)^2 + Z_1^2}, \quad (8)$$

$$s_1(t) = A_1 p_0 \left(t - \frac{2\mathbf{R}_1(t)}{c} \right) e^{-j2\omega_c \left(t - \frac{2\mathbf{R}_1(t)}{c} \right)} e^{j\varphi_1}. \quad (9)$$

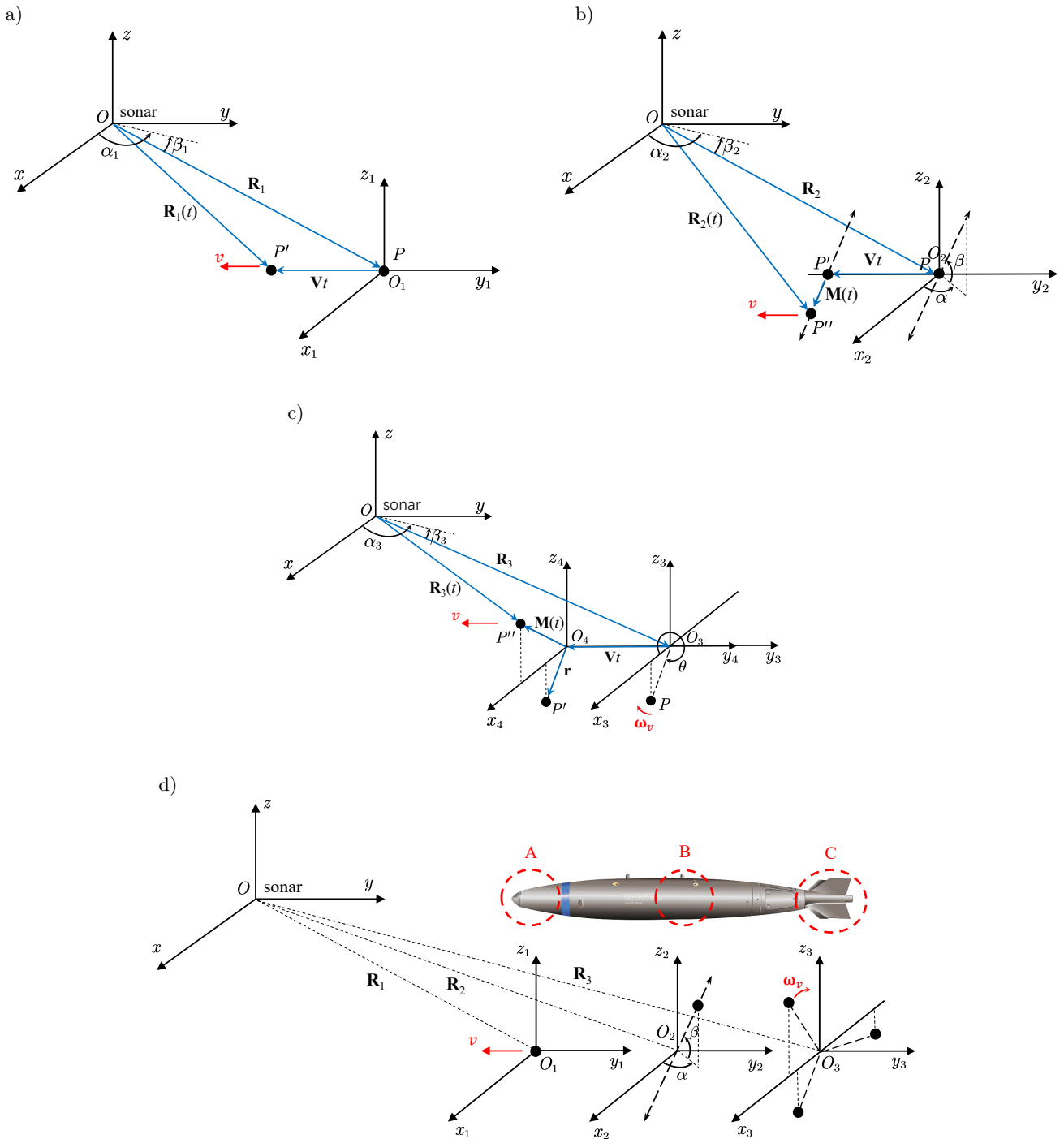


Fig. 2. The geometric relationship in the model: a) stationary high-light at position A; b) vibrating high-light at position B; c) rotating high-light at position C; d) geometric relationship between sonar and target.

It can be seen that there is no micro-Doppler; the only Doppler frequency shift is:

$$f_d = \frac{2f}{c} [\mathbf{V}^T \cdot \mathbf{n}_p] = \frac{2f}{c} (v \sin \alpha_1 \cos \beta_1). \quad (10)$$

For the vibrating highlight, as shown in Fig. 2b, assume that the highlight is initially located at position P , which corresponds to the origin O_2 in the target coordinate system (x_2, y_2, z_2) . The position vector

of the highlight in the sonar coordinate system (x, y, z) is denoted as $\mathbf{R}_2 = (X_2, Y_2, Z_2)^T$. The initial azimuth angle and pitch angle are represented as α_2 and β_2 , respectively. The unit vector in the radial direction from the sonar to the vibrating center O_2 of the target highlight takes the same form as Eq. (7).

The origin O_2 is the vibration center. The harmonic vibration is performed with frequency f_v and amplitude D_v . The azimuth angle of the vi-

bration direction is α , and the pitch angle is β . The unit vector of the vibration direction is $\mathbf{n}_v = (\cos \alpha \cos \beta, \sin \alpha \cos \beta, \sin \beta)^T$. In the form of simple harmonic vibration, the vibration distance is $D_t = D_v \sin(2\pi f_v t)$. And then the instantaneous distance is:

$$\begin{aligned} \mathbf{R}_2(t) &= \|\mathbf{R}_2 + \mathbf{V}t + D_t \cdot \mathbf{n}_v\| \\ &= [(X_2 + D_t \cos \alpha \cos \beta)^2 \\ &\quad + (Y_2 + vt + D_t \sin \alpha \sin \beta)^2 \\ &\quad + (Z_2 + D_t \sin \beta)^2]^{1/2}. \end{aligned} \quad (11)$$

Echo signal expression of the highlight is:

$$s_2(t) = A_2 p_0 \left(t - \frac{2\mathbf{R}_2(t)}{c} \right) e^{-j2\pi f \left(t - \frac{2\mathbf{R}_2(t)}{c} \right)} e^{j\varphi_2}. \quad (12)$$

The Doppler is the same as the stationary highlight, and the micro-Doppler is:

$$\begin{aligned} f_{md} &= \frac{2f}{c} \left[\frac{d}{dt} (D_v \sin(2\pi f_v t) \cdot \mathbf{n}_v) \right]^T \cdot \mathbf{n}_p \\ &= \frac{4\pi f_v f D_v}{c} \cos(2\pi f_v t) \\ &\quad \cdot [\cos(\alpha_2 - \alpha) \cos \beta_2 \cos \beta + \sin \beta_2 \sin \beta]. \end{aligned} \quad (13)$$

In summary, the micro-Doppler curve of a vibrating feature can be represented by a sinusoidal curve. The period of the micro-Doppler curve corresponds to the vibration period, and its amplitude is related to the vibration amplitude, vibration period, and the carrier frequency of the transmitted signal.

For rotating highlights, the three highlights differ only in their initial positions. By analyzing the general geometric relationship of a single highlight under motion, we can determine the motion features of three highlights. The rotation radius is l . The rotational angular velocity is $\boldsymbol{\omega} = (0, w, 0)$. The initial rotation angle of the rotation highlight at $t = 0$ is $\theta_i (i = 1, 2, 3)$. Therefore, the initial distance vector of the rotating highlights in the coordinate system (x_3, y_3, z_3) at $t = 0$ can be expressed as:

$$\mathbf{r}_i = (l \cos \theta_i, 0, l \sin \theta_i)^T. \quad (14)$$

For the motion analysis of a rotating highlight, its geometric relationship with the sonar system is depicted in Fig. 2c. At $t = 0$, the initial position of the target highlight is located at point P , and its initial rotation angle is denoted as θ . The initial position vector of the target highlight in the target coordinate system (x_3, y_3, z_3) is represented as $\mathbf{r} = (l \cos \theta, 0, l \sin \theta)^T$. The origin O_3 of the target coordinate system (x_3, y_3, z_3) has a position vector $\mathbf{R}_3 = (X_3, Y_3, Z_3)^T$ with respect to the sonar coordinate system (x, y, z) . The initial azimuth angle and pitch angle of the target coordinate system

are denoted as α_3 and β_3 , respectively. The unit vector in the radial direction from the sonar to the rotating center O_3 of the target highlight takes the same form as Eq. (7).

According to Rodrigues' formula (CHEN *et al.*, 2003), the instantaneous distance is:

$$\begin{aligned} \mathbf{R}_3(t) &= \|\mathbf{R}_3 + \mathbf{V}t + \mathbf{R}_t(t)\mathbf{r}\| \\ &= [(X_3 + l \cos \theta \cos \omega t + l \sin \theta \sin \omega t)^2 \\ &\quad + (Y_3 + vt)^2 \\ &\quad + (Z_3 - l \cos \theta \sin \omega t + l \sin \theta \cos \omega t)^2]^{1/2}. \end{aligned} \quad (15)$$

$\mathbf{R}_t(t)$ is the rotation matrix. The expression of the echo signal is obtained as:

$$s_3(t) = A_3 p_0 \left(t - \frac{2\mathbf{R}_3(t)}{c} \right) e^{-j2\omega_c \left(t - \frac{2\mathbf{R}_3(t)}{c} \right)} e^{j\varphi_3}. \quad (16)$$

When placing the target highlight and the sonar in the same plane, i.e., $X_3 = 0$, and applying an approximation method (CHEN, 2014), the specific expression for micro-Doppler can be derived as:

$$f_{md} = \frac{2f\omega l}{c} \sin \beta_3 \sin(\omega t + \theta_i). \quad (17)$$

In summary, the micro-Doppler curve of a rotating highlight follows a sinusoidal pattern, similar to that of a vibrating highlight. The period of the micro-Doppler curve corresponds to the rotational period of the motion. The amplitude of the micro-Doppler curve is influenced by the rotational radius, the rotation period, and the carrier frequency of the transmitted signal.

For the other two rotating highlights, their forms are similar. The final received echo signal form for a multi-highlight moving target is:

$$s(t) = \sum_{i=1}^5 s_i(t). \quad (18)$$

According to the traditional underwater target model (DONG *et al.*, 2013), the relative distances between the highlights of a target can result in different temporal distributions of their respective echoes. The relative distances between the highlights can also vary during the period of signal transmission due to the high-speed state of the target. Additionally, to capture finer micro-Doppler features, it is necessary to transmit detection signals with longer pulse widths, which ultimately leads to temporal overlap of the echoes from different highlights.

Since the initial moment corresponds to the time of signal transmission, the starting time of the echo signal is denoted as t_1 , and it is given by the equation:

$$t_1 = \tau_1 = \frac{2\mathbf{R}(t_1)}{c}, \quad (19)$$

where $\mathbf{R}(t_1)$ represents the position of the highlight when the sound wave illuminates it, which corresponds to the initial position in the aforementioned model. The termination time of the echo signal for the highlight is denoted as t_2 , and it is given by the equation:

$$t_2 = T + \tau_2 = T + \frac{2\mathbf{R}(t_2)}{c}. \quad (20)$$

The starting moment of the echo signal corresponds to the position of the highlight. It represents the position where the highlight is located after its motion, compensating for the positional changes caused by the time difference resulting from the relative distances between the highlights.

4. Simulation and analysis

In order to validate the accuracy and effectiveness of the model proposed in this paper, this section simulates the echo signals of moving targets under single-highlight and multi-highlight scenarios with micro-Doppler effects, based on the models established in Secs. 2 and 3. The short-time Fourier transform (STFT) is employed to obtain time-frequency spectrograms, which are then used to extract the motion features of the targets. This enables the estimation of target parameters.

4.1. Single-highlight micro-motion model simulation verification

Simulations and analyses were conducted for stationary highlights, vibrating highlights, and rotating highlights, with the initial moment defined as the time of signal transmission. Partial simulation parameter settings are shown in Table 1.

For the analysis of stationary highlights, the position vector of the target at the moment of sound wave illumination is calculated as $\mathbf{R}' = (0, 505.50, -200)^T$ m. Taking the initial position vector direction as the incident wave direction, the radial unit vector from the sonar to the target is $\mathbf{n}_p = \mathbf{R}' / \|\mathbf{R}'\|$, and the actual radial velocity component is $v = \mathbf{V}^T \cdot \mathbf{n}_p = 18.597$ m/s. The simulated echo signal pulse width is $T'_s = 0.4879$ s.

Derived from the actual radial velocity, it yields the Doppler factor $\delta = 0.0248$, which then compresses the pulse width to $(1 - \delta)T'_s = 0.4876$ s. This value is found to be consistent with the pulse width of the echo signal obtained in this paper's model. The same consistency is observed for vibrating highlights and rotating highlights.

The echo signal is subjected to STFT, resulting in a time-frequency distribution as shown in Fig. 3. The transmitted signal is a rectangular pulse signal, and the echo appears as a straight line on the time-frequency plot. By extracting the maximum value on the frequency axis at the middle moment, the Doppler frequency shift is $\xi = 741.925$ Hz. The radial velocity of the highlight translation is estimated to be $\hat{v} = 18.596$ m/s, which is consistent with the target radial velocity component.

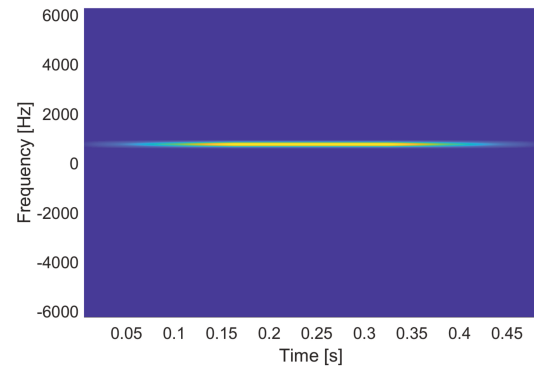


Fig. 3. STFT of the stationary highlight.

To analyze the vibrating highlights, the first step is to obtain the time-frequency representation. Then, peak extraction is performed on the time-frequency representation to obtain the micro-Doppler curve, as shown in Fig. 4.

The time difference between each maximum value is obtained from the micro-Doppler curve, resulting in the micro-Doppler period $\hat{T} = 0.0667$ s. The estimated vibration frequency $\hat{f} = \frac{1}{\hat{T}} = 15.024$ Hz is found to be in close agreement with the fundamental vibration frequency. Additionally, the micro-Doppler spread $\max f_{md} - \min f_{md} = 1382.6$ Hz is calculated by subtracting the minimum value from the maximum value

Table 1. Highlights simulation parameters.

Simulation parameters	Value
The initial position vector of each highlight	$\mathbf{R} = (0, 520, -200)^T$ m
The translational velocity vector of each highlight	$\mathbf{V} = (0, -20, 0)^T$ m/s
Vibration azimuth angle and pitch angle	$\alpha_v = 0, \beta_v = \frac{\pi}{2}$
Vibration frequency	$f_v = 10$ Hz
Vibration amplitude	$D_v = 0.5$ m
Rotational angular velocity vector	$\boldsymbol{\omega} = (0, 10\pi, 0)$ 1/s
Initial rotation angle	$\theta = 30^\circ$
Rotation radius	$l = 3$ m

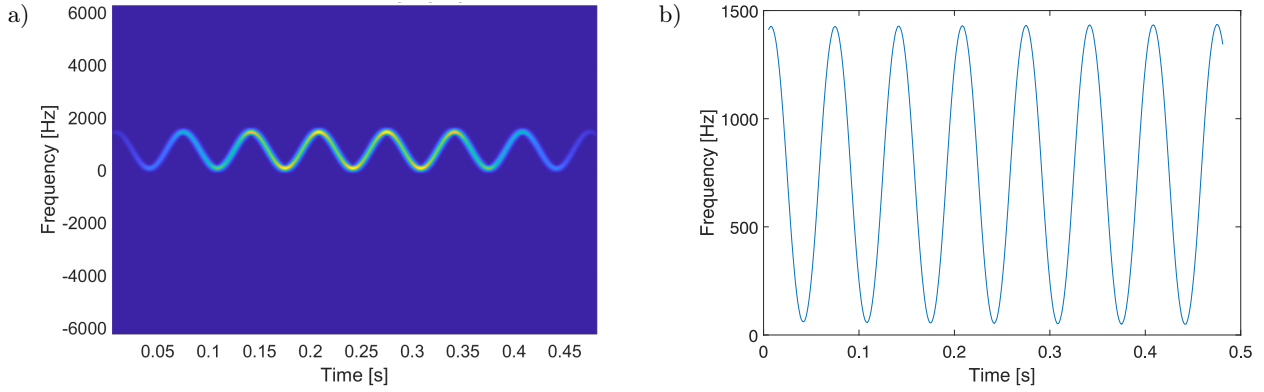


Fig. 4. STFT of the vibrating highlight (a) and the micro-Doppler curve of the vibrating highlight (b).

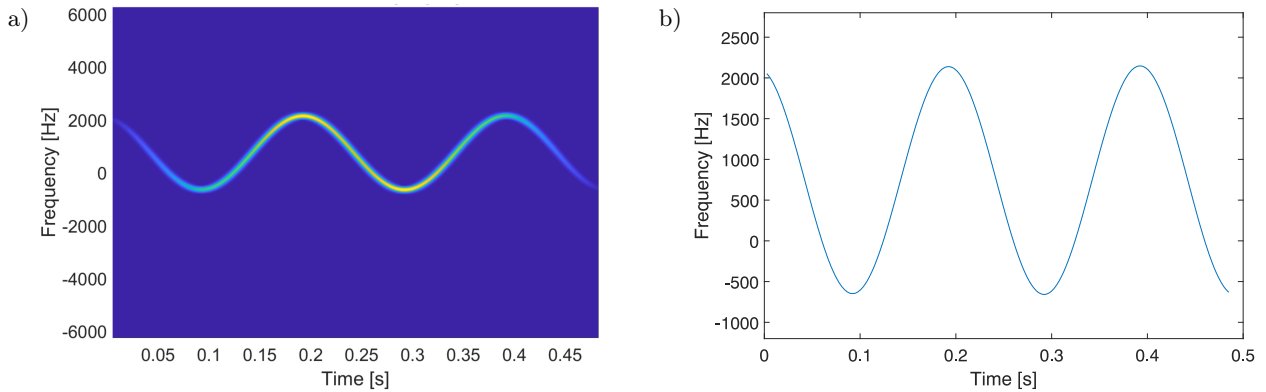


Fig. 5. STFT of the rotating highlight (a) and the micro-Doppler curve of the rotating highlight (b).

of the micro-Doppler curve. Then, the vibration amplitude estimation is $\widehat{D} = 0.497$ m, which is consistent with the vibration amplitude.

The same analysis is performed on the rotating highlight and the results are shown in Fig. 5. The time difference between each maximum value is obtained from the micro-Doppler curve, resulting in the micro-Doppler period $\widehat{T} = 0.1997$ s. The estimated angular velocity, $\widehat{\omega} = \frac{2\pi}{\widehat{T}} = 10.016\pi$ 1/s, is found to be in close agreement with the fundamental angular velocity. Additionally, the micro-Doppler spread $\max f_{md} - \min f_{md} = 2800.8$ Hz is calculated by sub-

tracting the minimum value from the maximum value of the micro-Doppler curve. And then the rotation radius estimation is $\widehat{l} = 3.017$ m, which is basically consistent with the rotation radius.

4.2. Simulation and analysis of multi-highlight moving target models

Simulation analysis is conducted on the multi-highlight model using the size parameters and motion parameters of a torpedo-like object. Some of the simulation parameters are set as shown in Table 2.

Table 2. Simulation parameters of the target.

Simulation parameters	Value
The initial position of stationary highlight in the head area of the target	$\mathbf{R}_1 = (0, 500, -200)^T$ m
The initial position of the vibrating highlight in the middle area of the target	$\mathbf{R}_2 = (0, 520, -200)^T$ m
The initial position of the rotating highlight in the tail area of the target	$\mathbf{R}_3 = (0, 540, -200)^T$ m
The translational velocity vector of each highlight	$\mathbf{V} = (0, -20, 0)^T$ m/s
Vibration azimuth angle and pitch angle	$\alpha_v = 0, \beta_v = \frac{\pi}{2}$
Vibration frequency	$f_v = 10$ Hz
Vibration amplitude	$D_v = 0.5$ m
Rotational angular velocity vector	$\boldsymbol{\omega} = (0, 10\pi, 0)$ 1/s
Initial rotation angle	$\theta = 30^\circ$
Rotation radius	$l = 3$ m
The initial rotation angle of each rotating highlight	$\theta_1 = 30^\circ, \theta_2 = 150^\circ, \theta_3 = 270^\circ$

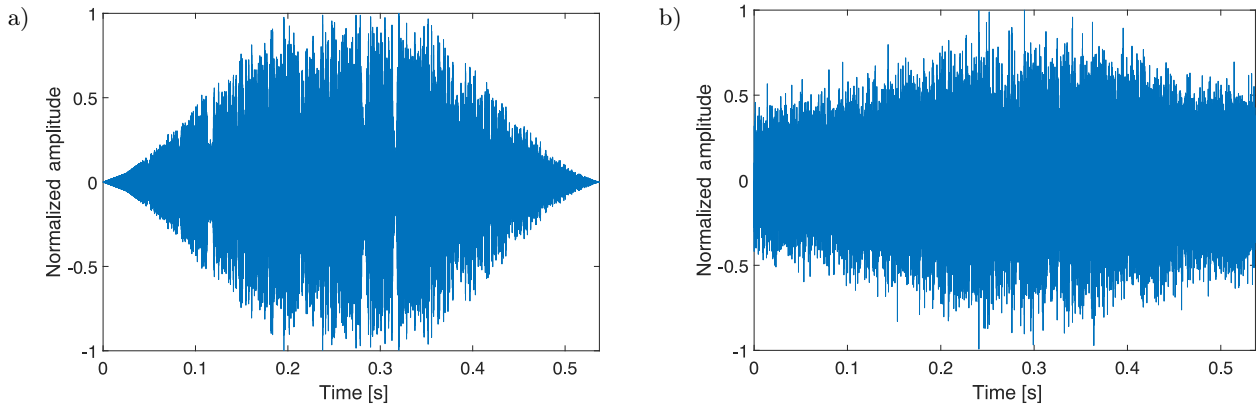


Fig. 6. Final received signal simulation process: a) echo in time domain; b) received signal in time domain.

Taking into account the received echo signals in real underwater environments, it should be noted that these signals are not entirely comprised of valid information due to the presence of environmental noise and reverberation interference in marine environments. The actual received signal is a mixture of the echo signal, noise, and reverberation. By considering the spectral characteristics of marine environmental noise and Gaussian white noise in the frequency domain, the required environmental noise is simulated (HAN *et al.*, 2020). The ocean reverberation is simulated using a unit scattering model (LI, LIU, 2016). The simulated echo time-domain sequence is shown in Fig. 6a. The noise and reverberation are then superimposed on the echo, resulting in the final received signal time-domain sequence as shown in Fig. 6b. The signal-to-noise ratio (SNR) of the final received signal is -1.81 dB, and the signal-to-reverberation ratio (SRR) is -2.51 dB.

The final received signal is processed as follows: first, the analytic signal of the echo signal is obtained, and then it is multiplied by the complex conjugate of the transmitted signal to obtain the baseband signal. Finally, the STFT is applied to the baseband signal, resulting in the time-frequency distribution shown in Fig. 7. By processing the echo signal into a baseband signal, the energy of the reverberation is concentrated

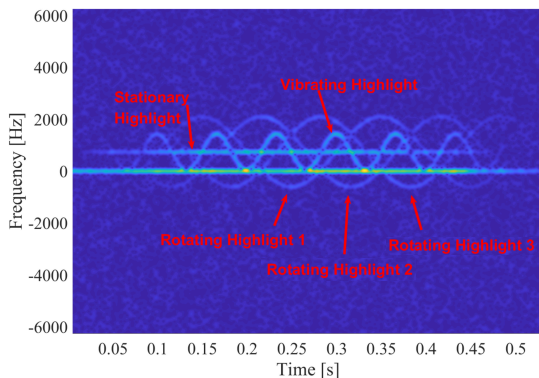


Fig. 7. STFT of the echo.

at frequency 0. The bright straight line above the reverberation represents the energy distribution of the stationary highlight at the target's head, characterized by relatively large energy and smaller amplitude. The micro-Doppler curves with larger amplitudes and smaller magnitudes represent the energy distribution of the vibrating highlights at the target's midsection. The three micro-Doppler curves with the highest amplitudes correspond to the energy distribution of the three rotating highlights at the target's tail.

From the time-frequency distribution graph, we can observe that the approximate time difference between the peaks of the micro-Doppler curves for the vibrating highlights is between 0.06 and 0.07 s. This allows us to make a rough estimation of the vibration frequency in the range of 14 to 16 Hz. On the other hand, the approximate time difference between the peaks of the micro-Doppler curves for the rotating highlights is around 0.2 s. This suggests a rough estimation of the rotational angular frequency at approximately 5 Hz.

By modifying the parameters of the micro-motion, we can observe changes in the time-frequency distribution of the target echo. Based on the aforementioned simulation parameters, we change the vibration amplitude of the vibrating highlight, denoted as $D_v = 1$ m, and the rotation radius of the rotating highlight, denoted as $l = 5$ m. The resulting STFT of the echo is shown in Fig. 8. Then, keeping the amplitude and rotation radius unchanged, we modify the vibration frequency of the vibrating highlight ($f_v = 20$ Hz) and the rotation frequency of the rotating highlight ($f_r = 8$ Hz). The resulting STFT of the echo is shown in Fig. 9.

It is observed that the time-frequency distribution exhibits significant changes compared to the previous simulation results. Increasing the vibration amplitude and rotation radius leads to a larger micro-Doppler spread in the echo. Similarly, increasing the vibration frequency and rotation frequency results in a larger micro-Doppler period and an increased micro-Doppler spread in the echo.

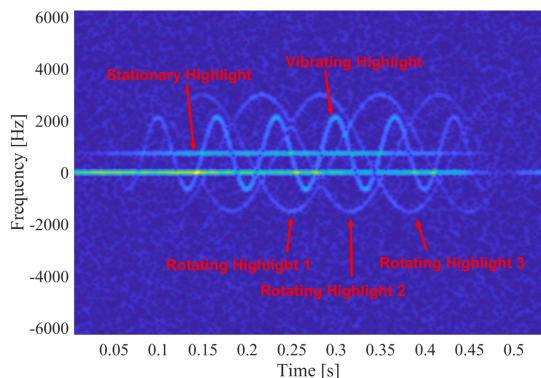


Fig. 8. STFT of the echo with modified vibration amplitude and rotation radius.

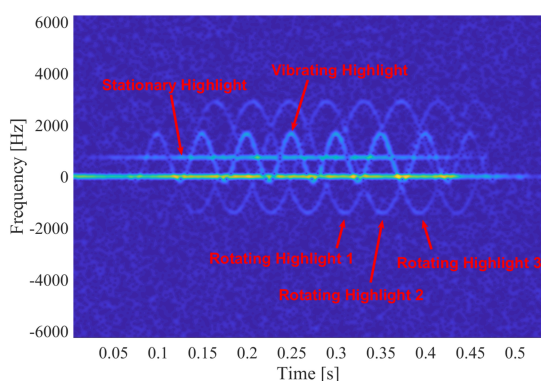


Fig. 9. STFT of the echo with modified vibration frequency and rotation angular velocity.

This indicates that in practical scenarios, the micro-Doppler features are influenced by the micro-motion parameters of the target. Different micro-motion forms of the target or different micro-motion states within the same micro-motion form will result in distinct patterns in the time-frequency domain. Additionally, in theoretical derivations, the micro-Doppler is also influenced by parameters such as the target's initial position and the carrier frequency of the transmitted signal.

Therefore, micro-Doppler can be utilized as a motion feature for target classification and recognition, while the Doppler frequency shift is primarily used to extract the target's radial velocity and can also serve as a motion feature.

5. Conclusion

This paper investigated the underwater motion feature models for the multi-highlight targets at high speed based on highlight model and the micro-Doppler effect. Firstly, the positional variations of the target highlights were incorporated into the model, and a single-highlight model was established for compound motion patterns. Subsequently, a motion target model was proposed for multiple highlights with micro-

Doppler effects, and the effectiveness of the model was validated through motion parameter estimation using simulated results and the simulation of target echoes in real underwater environments.

The research results demonstrate that the echo pulse width of the composite motion single-highlight model coincides with the pulse width compression (or expansion) caused by translational velocity. Moreover, its micro-doppler characteristics can be fully manifested in the time-frequency distribution, and precise micro-motion parameters such as vibration frequency and rotational velocity can be accurately extracted from the time-frequency distribution. These findings validate the accuracy of the model and its superior representation of motion characteristics compared to traditional underwater point target models.

Additionally, the multi-highlight moving target model addresses the limitations of the single-highlight model in describing complex body targets. The echo simulation results based on this model fully demonstrate the effects of echo superposition caused by differences in the positions of multiple points and translational velocity in the time-frequency distribution, confirming the effectiveness of the model proposed in this study. Furthermore, variations in micro-motion parameters also lead to noticeable differences in the time-frequency distribution, and a rough estimation of the target's micro-motion parameters can be obtained from the time-frequency distribution. This indicates that micro-Doppler can serve as a motion feature for the target. The proposed model in this study provides a theoretical foundation and approach for the investigation of underwater moving targets, serving as a reference for further exploration of the motion features of underwater targets.

References

1. CHEN G. (2014), *Micro-Doppler signature analysis of radar targets and its applications* [in Chinese], Ph.D. Thesis, Xidian University in Xi'an, China, doi: [10.7666/d.D725864](https://doi.org/10.7666/d.D725864).
2. CHEN V.C., LI F., HO S.S., WECHSLER H. (2003), Analysis of micro-Doppler signatures, [in:] *IEE Proceedings-Radar, Sonar and Navigation*, **150**(4): 271–276, doi: [10.1049/ip-rsn:20030743](https://doi.org/10.1049/ip-rsn:20030743).
3. CLEMENTE C., BALLERI A., WOODBRIDGE K., SORAGHAN J.J. (2013), Developments in target micro-Doppler signatures analysis: Radar imaging, ultrasound and through-the-wall radar, *EURASIP Journal on Advances in Signal Processing*, **2013**: 47, doi: [10.1186/1687-6180-2013-47](https://doi.org/10.1186/1687-6180-2013-47).
4. DONG Z., LI Y., CHEN X. (2013), Submarine echo simulation method based on highlight model [in Chinese], *Computer Simulation*, **30**(6): 38–41, doi: [10.3969/j.issn.1006-9348.2013.06.009](https://doi.org/10.3969/j.issn.1006-9348.2013.06.009).
5. GAO H., XIE L., WEN S., KUANG Y. (2010), Micro-Doppler signature extraction from ballistic target with

- micro-motions, *IEEE Transactions on Aerospace and Electronic Systems*, **46**(4): 1969–1982, doi: [10.1109/TAES.2010.5595607](https://doi.org/10.1109/TAES.2010.5595607).
6. GONG Z., LI C., JIANG F., ZHENG J. (2020), AUV-aided localization of underwater acoustic devices based on Doppler shift measurements, *IEEE Transactions on Wireless Communications*, **19**(4): 2226–2239, doi: [10.1109/TWC.2019.2963296](https://doi.org/10.1109/TWC.2019.2963296).
 7. HAN L., FENG C. (2020), Micro-Doppler-based space target recognition with a one-dimensional parallel network, *International Journal of Antennas and Propagation*, **2020**: 8013802, doi: [10.1155/2020/8013802](https://doi.org/10.1155/2020/8013802).
 8. HAN M., WANG C., SUN Q., WANG W., LU Y. (2020), Measurement and analysis of ambient noise in the South China Sea based on underwater acoustic buoy [in Chinese], *Journal of Applied Acoustics*, **39**(4): 536–542, doi: [10.11684/j.issn.1000-310X.2020.04.006](https://doi.org/10.11684/j.issn.1000-310X.2020.04.006).
 9. HANIF A., MUAZ M., HASAN A., ADEEL M. (2022), Micro-Doppler based target recognition with radars: A review, *IEEE Sensors Journal*, **22**(4): 2948–2961, doi: [10.1109/JSEN.2022.3141213](https://doi.org/10.1109/JSEN.2022.3141213).
 10. KASHYAP R., SINGH I., RAM S.S. (2015), Micro-Doppler signatures of underwater vehicles using acoustic radar, [in:] *2015 IEEE Radar Conference (Radar-Con)*, pp. 1222–1227, doi: [10.1109/RADAR.2015.7131181](https://doi.org/10.1109/RADAR.2015.7131181).
 11. KIM Y., LING H. (2009), Human activity classification based on micro-Doppler signatures using a support vector machine, *IEEE Transactions on Geoscience and Remote Sensing*, **47**(5): 1382–1337, doi: [10.1109/TGRS.2009.2012849](https://doi.org/10.1109/TGRS.2009.2012849).
 12. KIM Y., MOON T. (2016), Human detection and activity classification based on micro-Doppler signatures using deep convolutional neural networks, *IEEE Geoscience and Remote Sensing Letters*, **13**(1): 8–12, doi: [10.1109/LGRS.2015.2491329](https://doi.org/10.1109/LGRS.2015.2491329).
 13. KOU S., FENG X. (2022), Angle-micro-Doppler frequency image of underwater target multi-highlight combining with sparse reconstruction, *Applied Acoustics*, **188**: 108563, doi: [10.1016/j.apacoust.2021.108563](https://doi.org/10.1016/j.apacoust.2021.108563).
 14. KULHANDJIAN H., RAMACHANDRAN N., KULHANDJIAN M.K., D'AMOURS C. (2020), Human activity classification in underwater using sonar and deep learning, [in:] *Proceedings of the 14th International Conference on Underwater Networks & Systems*, pp. 1–5, doi: [10.1145/3366486.3366509](https://doi.org/10.1145/3366486.3366509).
 15. LI S., LIU S. (2016), A modeling and simulation based on k-distribution model [in Chinese], *Ship Science and Technology*, **38**(s1): 158–161, doi: [10.3404/j.issn.1672-7619.2016.S1.029](https://doi.org/10.3404/j.issn.1672-7619.2016.S1.029).
 16. SAFFARI A., ZAHIRI S.-H., KHISHE M. (2023), Automatic recognition of sonar targets using feature selection in micro-Doppler signature, *Defence Technology*, **20**: 58–71, doi: [10.1016/j.dt.2022.05.007](https://doi.org/10.1016/j.dt.2022.05.007).
 17. TANG W. (1994), Highlight model of echoes from sonar targets, *Acta Acustica*, **19**(2): 92–100.
 18. TANG Y., WANG X., LI H., GAO C., MIAO X. (2020), Experimental research on interior field noise and the vibration characteristics of composite reinforced sheet-beam structures, *Applied Acoustics*, **160**: 107154, doi: [10.1016/j.apacoust.2019.107154](https://doi.org/10.1016/j.apacoust.2019.107154).
 19. WANG Z., REN A., ZHANG Q., ZAHID A., ABBASI Q.H. (2023), Recognition of approximate motions of human based on micro-Doppler features, *IEEE Sensors Journal*, **23**(11): 12388–12397, doi: [10.1109/JSEN.2023.3267820](https://doi.org/10.1109/JSEN.2023.3267820).
 20. WU Y., LUO M., LI S. (2022), Measurement and extraction of micro-Doppler feature of underwater rotating target echo, [in:] *OCEANS 2022 – Chennai*, pp. 1–5, doi: [10.1109/OCEANSChennai45887.2022.9775247](https://doi.org/10.1109/OCEANSChennai45887.2022.9775247).
 21. XU L. (2016), *Study on Doppler parameter estimation of underwater acoustic signal and its application* [in Chinese], Ph.D. Thesis, Northwestern Polytechnical University in Xi'an, China, doi: [10.7666/d.D01304090](https://doi.org/10.7666/d.D01304090).
 22. YANG Y., FAN J., WANG B. (2023), Research on scattering feature extraction of underwater moving cluster targets based on the highlight model, *Archives of Acoustics*, **48**(2): 235–247, doi: [10.24425/aoa.2023.145235](https://doi.org/10.24425/aoa.2023.145235).
 23. ZHANG B., HU Y., WANG H., ZHUANG Z. (2018), Underwater source localization using TDOA and FDOA measurements with unknown propagation speed and sensor parameter errors, *IEEE Access*, **6**: 36645–36661, doi: [10.1109/ACCESS.2018.2852636](https://doi.org/10.1109/ACCESS.2018.2852636).
 24. ZHANG R., WANG Y., YE H. C., LU X. (2023), Precission parameter estimation of warhead with fins based on micro-Doppler effect and radar network, *IEEE Transactions on Aerospace and Electronic Systems*, **59**(1): 443–459, doi: [10.1109/TAES.2022.3182635](https://doi.org/10.1109/TAES.2022.3182635).
 25. ZHAO Y., SU Y. (2023), Estimation of micro-Doppler parameters with combined null space pursuit methods for the identification of LSS UAVs, *IEEE Transactions on Geoscience and Remote Sensing*, **61**: 1–11, doi: [10.1109/TGRS.2023.3264643](https://doi.org/10.1109/TGRS.2023.3264643).